White Rose Research Online

eprints@whiterose.ac.uk
https://eprints.whiterose.ac.uk
Universities of Leeds, Sheffield and York

Deposited via The University of Sheffield.

White Rose Research Online URL for this paper:
https://eprints.whiterose.ac.uk/id/eprint/105171/

Version: Accepted Version

Article:
Lin, L., Miao, N., Wen, Y. et al. (2016) Sulphur-Depleted Monolayered Molybdenum Disulfide Nanocrystals for Superelectrochemical Hydrogen Evolution Reaction. ACS Nano, 10 (9). pp. 8929-8937. ISSN: 1936-0851

https://doi.org/10.1021/acsnano.6b04904

This document is the Accepted Manuscript version of a Published Work that appeared in final form in ACS Nano, copyright © American Chemical Society after peer review and technical editing by the publisher. To access the final edited and published work see http://dx.doi.org/10.1021/acsnano.6b04904.

Reuse
Items deposited in White Rose Research Online are protected by copyright, with all rights reserved unless indicated otherwise. They may be downloaded and/or printed for private study, or other acts as permitted by national copyright laws. The publisher or other rights holders may allow further reproduction and re-use of the full text version. This is indicated by the licence information on the White Rose Research Online record for the item.

Takedown
If you consider content in White Rose Research Online to be in breach of UK law, please notify us by emailing eprints@whiterose.ac.uk including the URL of the record and the reason for the withdrawal request.

UNIVERSITY OF LEEDS
University of Sheffield
UNIVERSITY of York

Sulphur Depleted Monolayered Molybdenum Sulfide Nanocrystals for Super Electrochemical Hydrogen Evolution Reaction

Liangxu Lin,[†,‡] Naihua Miao,[§,∥] Yan Wen,[†] Shaowei Zhang,[†] Philippe Ghosez,[§] Zhimei Sun,[∥] and Dan A. Allwood*[‡]*

[†]College of Engineering, Mathematics and Physical Sciences, University of Exeter, Exeter, EX4 4QL, UK

[‡]Department of Materials Science and Engineering, University of Sheffield, Sheffield, S1 3JD, UK

[§]Theoretical Materials Physics, Institut de Physique, Université de Liège, Liège, B-4000, Belgium

[∥]Center for Integrated Computational Materials Engineering & School of Materials Science and Engineering, Beihang University, Beijing, 100191, China

KEYWORDS. Monolayered Molybdenum Sulfide, Nanocrystals, Hydrogen Evolution Reaction, Electrochemical

ABSTRACT. Catalytically-driven electrochemical hydrogen evolution reaction (HER) of monolayered molybdenum sulfide (MoS_2) is usually highly supressed by the scarcity of edges and low electrical conductivity. Here, we show how the catalytic performance of MoS_2 monolayers can be improved dramatically by catalyst size reduction and surface sulphur (S)

depletion. Monolayered MoS_2 nanocrystals (NCs) (2-25 nm) produced *via* exfoliating and disintegrating their bulk counterparts showed improved catalysis rates over monolayer sheets because of their increased edge ratios and metallicity. Subsequent S depletion of these NCs further improved the metallicity and made Mo atoms on the basal plane become catalytically active. As a result, the S-depleted NCs with low mass (~1.2 μg) showed super high catalytic performance on HER with a low Tafel slope of ~29 mV/decade, overpotentials of 60-75 mV, high current densities J_x (where x is in mV) of j_{150} = 9.64 mA.cm^{-2}, and j_{200} = 52.13 mA.cm^{-2}. We have found that higher production rates of H_2 could not be achieved by adding more NC layers since HER only happens on the topmost surface and the charge mobility decreases dramatically. These difficulties can be largely alleviated by creating a hybrid structure of NCs immobilized onto three-dimensional (3D) graphene to provide a very high surface exposure of the catalyst for electrochemical HER, resulting in very high current densities of J_{150} = 49.5 mA.cm^{-2} and J_{200} = 232 mA.cm^{-2} with ~14.3 μg NCs. Our experimental and theoretical studies show how careful design and modification of nanoscale materials/structures can result in highly efficient catalysis. There may be considerable opportunities in the broader family of transition metal dichalcogenides beyond just MoS_2 to develop highly efficient atomically thin catalysts. These could offer cheap and effective replacement of precious metal catalysts in clean energy production.

To address pressing energy and environmental crises affecting our society, electrochemical HER is considered as one of the promising techniques to produce clean energy with sustainable high production.[1-8] The most effective catalysts today are precious metals (*e.g.* Pt) but their scarcity and prohibitive expense limits their practical implementation. Recent developments have emphasized that molybdenum disulphide (MoS_2) based materials may offer cheaper and more

readily available catalysts.[1-10] However, the catalytic performance of layered MoS_2 structures is highly restricted by the scarcity of metal edges[2,5,8] and the low electron transport efficiency in multilayered phases (catalytic activity decreases by a factor of ~4.5 with each additional layer).[7] Improvements in MoS_2 catalytic performance have been made by increasing edge exposures (*e.g.* surface structure engineering),[3] improving electron transport efficiency (*e.g.* formation of monolayers, 1T metallic monolayers on graphite, and nanoparticles/NPs binding with highly conductive graphene),[11-14] and modulating the electronic structure *via* chemical doping.[15,16] Nevertheless, the majority of metal atoms in these particles remain within the basal plane away from particle edges, which unfortunately are catalytically inactive.[2,5,8] Large production of hydrogen (H_2) [with high exchange current density (j) at low overpotentials] also cannot be simply achieved using multiple layers of catalyst, which is rarely recognized (*i.e.* the stacking of monolayers also dramatically decreases catalytic performance, which will be confirmed in Figure 3d and Figure 5b).

To overcome these technical challenges, here we demonstrate a super electrochemical HER catalyst based on the size reduction and sulphur (S) depletion on MoS_2 monolayers. Compared to 3D nanoparticles and large monolayered sheets, monolayered NCs have a greatly increased density of catalytically active metal edges (*e.g.* over factor 100 times greater edge density for 10 × 10 nm NCs *vs* 1 × 1 μm sheets, see Figure S1a, Supporting Information). We have achieved a similar improvement by surface S-depletion to activate metal sites on the basal plane for catalysis (Figure S1a) following previous theoretical predictions.[17] The formed NCs are further dispersed and loaded on thermally expanded graphene oxide (EG, with 3D porous graphene-like structure) to alleviate the stacking of NCs and achieve high H_2 production.

RESULTS AND DISCUSSION

Preparation and Characterization of Monolayered MoS_2 NCs. We developed a method for fabrication of S-depleted Mo-S NCs, and characterized as-prepared NCs with a variety of techniques to understand their structure. Due to the layered structure of bulk 2H-MoS_2, monolayered MoS_2 NCs (2-25 nm width, average size ~12.9 nm, yield of ~ 31 wt%) were prepared with a simple and safe method we established previously with monolayered NC fabrication of graphene,[18] tungsten disulfide (2H-WS_2),[19] and hexagonal boron nitride (hBN).[20] Here, this preparation required the rapid delamination of potassium-intercalated MoS_2 (K-MoS_2) flakes in EtOH (ethanol) then with H_2O under ultrasonication. The intercalation reaction of layered materials was also demonstrated well by Jacobson *et al*.[21] The reaction between K-MoS_2 and its solvent (*e.g.* EtOH/H_2O) generates hydrogen gas and simultaneously exfoliates and disintegrates the thin layers to monolayered NCs under ultrasonication. Monolayered 2H-MoS_2 NCs were formed with a high yield (31 wt%) (Figure S1-4), an average width of ~12.9 nm and high crystallinity (Figure 1a; Figure S2e-g and Figure S4) with over 90% having a thickness of ~0.9 nm (Figure S2f), corresponding to that of monolayers.[22] As-prepared NCs were stable and highly luminescent with a quantum yield of 7.9% using Rhodamine B as a reference (Figure S1h and Table S1, Supporting Information), further revealing the semiconducting 2H structure. We found two ultraviolet/visible (UV/Vis) absorption peaks of 2H-MoS_2 NCs at 470 (2.64 eV) and 390 nm (3.12 eV) (Figure S5a), which were at noticeably shorter wavelengths than for monolayered MoS_2 sheets.[22] Nevertheless, the absorption peaks A and B of the NCs here were close to those found using MoS_2 nanoclusters approximately 4.0-4.5 nm in diameter, which had been previously assigned to the excitonic absorption peaks A and B (at the K point) of the first Brillouin zone.[23]

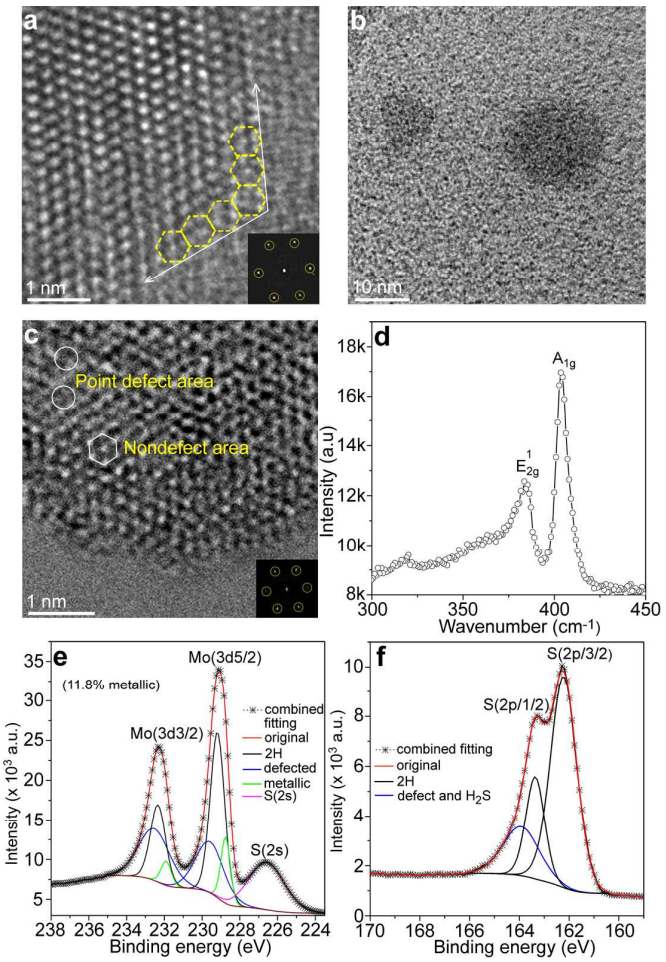

Figure 1. (a) HRTEM image of the edge of initial NCs before S-depletion. The inset is the related fast Fourier transform (FFT) pattern, confirming hexagonal and zigzag edge structures of the NC. (b,c) HRTEM images of the S-depleted $MoS_{1.65}$ NCs. The FFT pattern (inset) in (c) reveals hexagonal crystal structure of the NC. (d) Raman spectrum of S-depleted $MoS_{1.65}$ NCs. (e,f) Mo(3d) and S(2p) XPS of S-depleted $MoS_{1.65}$ NCs. Full-width-at-half-maximum (FWHM) of the Mo (3d) peak is larger than in the cases of other monolayered MoS_2 sheets, due to the S-depletion-induced crystal disorder.[25]

Preparation and Characterization of S-depleted Monolayered Mo-S NCs. We treated the 2H-MoS_2 NCs with a cation exchange resin (see Method and Materials), which generated smelly H_2S gas and partially depleted S from the NCs. The initially faintly colored 2H-MoS_2 NCs suspension also changed to a brown suspension with increased visible absorption upon S-

depletion (Figure S5a-b). X-ray photoelectron spectroscopy (XPS) measurements showed that the S-depleted NCs had a chemical composition of $MoS_{1.65}$ (Figure S5c). Nevertheless, the diameter of the $MoS_{1.65}$ NCs (12.5±0.5 nm) (Figure S5d-e) remained close to that of the initial MoS_2 NCs. High-resolution transmission electron microscopy (HRTEM) showed that pre-treated MoS_2 NCs were highly crystallized without any clear surface S vacancies and with clear, terminated edges (Figure 1a; Figure S4d-f). However, we only found rough edges and low crystallinity of S-depleted NCs, commonly with point defects (S vacancies) (Figure 1b-c).

Despite these observations of crystal ordering, Raman spectroscopy of the S-depleted NCs showed that the underlying 2H crystal structure of the original NCs remained (Figure 1d, which is consistent with the FFT pattern in Figure 1c), with E^1_{2g} and A_{1g} Raman modes at 383.6 and 403.7 cm^{-1}, respectively, corresponding to those of 2H-MoS_2.[22] The observation of the in-plane-vibrational mode at 383.6 cm^{-1} also suggested that the trigonal prismatic coordination of pristine MoS_2 flakes, absent from the metastable octahedral coordination phase, had been preserved.[24] XPS spectra of the $MoS_{1.65}$ NCs (Figure. 1e-f) show that both the Mo(3d) (at 232.3 and 229.1 eV) and S(2p) (at 163.3 and 162.3 eV) peaks are asymmetric and broad due to crystal defects and metallic sites. The absence of prominent peaks at around 236 eV and 168-170 eV means that oxidation of Mo (Mo^{6+}) and S was minimal.[22,25] Fitting the XPS data with Gaussian peaks representative of 2H-MoS_2 structure, gave strong contributions from Mo $3d_{3/2}$ (232.6 eV), Mo $3d_{5/2}$ (229.6 eV), S 2p (163.9 eV) in defect-containing Mo-S NCs.[22,25] There are also two Mo (3d) peaks at 231.8 and 228.7 eV, which can be attributed to metallic phase on $MoS_{1.65}$ NCs (shifted down to lower binding energies, depending on S vacancy densities).[25] These metallic phases were also present in pure NCs without S-depletion (Figure S3b), and unlikely to be due to the 1T octahedral coordination phase since MoS_2 NCs were highly luminescent and stable

(Raman investigations also suggested strong 2H vibration modes of S-depleted NCs, Figure 1d). To further understand this metallic feature, we used density functional theory to calculate the electronic band structure of NCs before and after S-depletion (details about the calculation methods and models are given in Supporting Information). The overall electronic density of states (DOS) of MoS_2 NCs before S-depletion (Figure 2a, pure NC) appears to be metallic but closer examination reveals that it in fact combines metallic and semiconducting characteristics. The metallic character is limited to the NC edge and near-edge regions while the inner NC core remains semiconducting, similarly to extended MoS_2 monolayers. Upon S-depletion, NCs become more metallic at both the monolayer surface and edge (Figure 2a). Besides, defect states below the bottom of the conduction band are also formed, which, in principle, improves charge mobility of NCs.[26] These defect states originate mainly from the *p* and *d* orbitals of Mo and the *p* orbital of S atoms (Figure 2b). To improve the understanding of these metallic and semiconducting regions, a simple model of the NCs is prepared, as shown in Figure 2c.

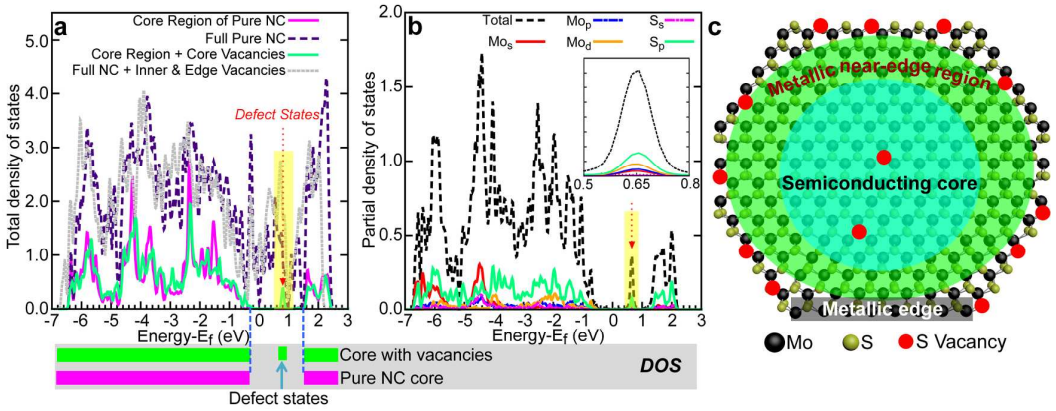

Figure 2. (a) Calculated DOS of MoS_2 in the form of a NC with/without S-vacancies in the core (c-NC) and/or edge region (e-NC), and the DOS of an entire S-depleted NC. The DOS unit is states.eV^{-1}f.u.$^{-1}$ (f.u.: formula unit). (b) Decomposition of the total DOS of MoS_2 c-NC with S-vacancies (S-depletion) in the core and edge regions into partial DOS of the Mo and S orbitals. The inset is the enlarged local area of the partial DOS from 0.5 eV to 0.8 eV. (c) Diagram of the S-depleted NCs, showing metallic edge, near edge regions and semiconducting core.

Catalytic Performance of Monolayered MoS_2 NCs. Upon the above preparations, we initially estimated the catalytic performance of MoS_2 NCs using approximately 4.78 μg (67.7 $\mu g.cm^{-2}$) immobilized material (see Method and Materials, and Captions of Figure S5f-g for the mass confirmation) for HER by the three-electrode technique (working electrode: glassy carbon, 3 mm diameter; counter electrode: Pt; reference electrode: Ag/AgCl, 1M KCl) in 0.5M aqueous H_2SO_4 (pH close to 0) at room temperature and a scan rate of 50 $mV.s^{-1}$. The polarization curve (all *iR* corrected in this report) of exchange current density, *j*, against voltage, *V*, of the catalyst (Figure 3a, including the polarization curve of Pt electrode for comparison) provides an onset overpotential (η) of 120-140 mV *vs* reversible hydrogen electrode (RHE). HER using an identical mass of bulk MoS_2 raw material was negligible. The Tafel slope (Figure 3b) of 51 mV/decade obtained from this polarization curve is much lower than that (~339 mV/decade) for bulk MoS_2. It is also already much lower than the values reported for many nanosized MoS_2 materials, *e.g.* 140-145 mV/decade for monolayered sheets,[7] 61 mV/decade for monolayered MoS_2 nanoflakes on gold foil,[11] 55-67 mV/decade for O-doped ultrathin MoS_2 nanosheets,[26] and comparable to those reported for surface aligned/engineered MoS_2 nano films (44-84 mV/decade)[4] and amorphous MoS_2 thin film (47-51 mV/decade).[27] This suggests an enhanced electrocatalytic performance due to size and thickness reduction and high catalytic activity of monolayered MoS_2 NCs. The catalytic performance improvement from bulk to monolayered MoS_2 NCs is understandable, as the reduction of thickness and size improves the number of catalytically active sites (Figure S1a) and charge mobility (electron hopping efficiency decreases by a factor of ~4.5 with each additional layer).[7]

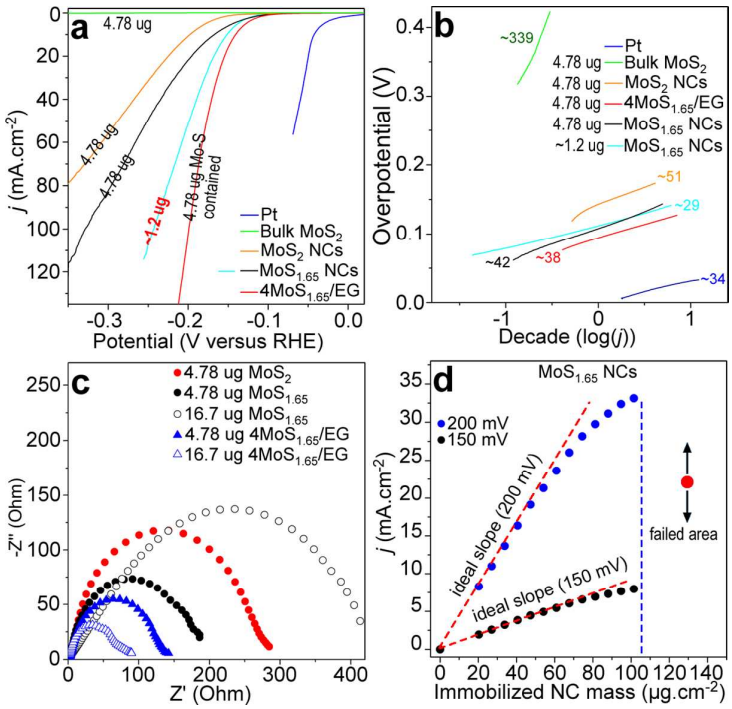

Figure 3. (a) Polarization curves and (b) Tafel plots (obtained from polarization curves) of bulk MoS_2, MoS_2 NCs, S-depleted $MoS_{1.65}$ NCs, $4MoS_{1.65}$/EG catalysts and Pt electrode. (c) Nyquist plots showing EIS response with real (Z') and imaginary (Z'') impedance components of MoS_2, $MoS_{1.65}$, and $4MoS_{1.65}$/EG catalysts (the masses of Mo-S NCs contained in catalysts are shown in the figure). (d) Plots of current density at 150 mV (j_{150}) and 200 mV (j_{200}) against catalyst mass loading of pure $MoS_{1.65}$ NCs. j_{200} and j_{150} of bare glassy electrode were negligible (Figure S6a) and set as 0 $mA.cm^2$.

Catalytic Performance of S-Depleted Monolayered Mo-S NCs. Similar analysis on the S-depleted $MoS_{1.65}$ NCs with an identical mass (4.78 μg, Figure 3a-b) showed η = 70-95 mV and a Tafel slope of ~42 mV/decade, representing a significant improvement over pristine MoS_2 NCs and most MoS_2 based catalysts.[1,4,7,11,14] A 3000 cycle durability test of monolayered $MoS_{1.65}$ NCs showed negligible loss of electrochemical current (Figure S5i), demonstrating their stability for electrochemical HER in acid media. The S-depletion of MoS_2 NCs to form $MoS_{1.65}$ NCs also decreased charger transfer resistances (R_{ct}) from ~300 Ω (MoS_2 NCs) to ~200 Ω at 80 mV overpotential with identical mass (Figure 3c). The electrochemical current density obtained with

4.78 μg of $MoS_{1.65}$ NCs at potentials of 200 mV (j_{200}) and 150 mV (j_{150}) were then calculated as 26.01 and 6.05 $mA.cm^{-2}$, respectively, which were much improved from NCs without S-depletion (Figure 3a). We found that much better catalytic performance of S-depleted NCs can be achieved with fewer (~1.2 μg) and highly dispersed NCs (NCs were diluted with EtOH to 4 times and sonicated for 1 minute before immobilization). In this case, a very low Tafel slope of ~29 mV/decade (lower than Pt electrode, 34 mV/decade), η = 60-75 mV, j_{150} = 9.64 $mA.cm^{-2}$, and j_{200} = 52.13 $mA.cm^{-2}$ were achieved (Figure 3a,b), representing super high catalytic activity of the S-depleted Mo-S NCs per μg (see Table S2 for more information). We consider that the catalytic performance of NCs was highly affected by the immobilization method, particularly the stacking of NCs, which will be further discussed in detail below.

Difficulties in Improving Catalytic Performance with More S-Depleted NCs Immobilized. For efficient electrochemical HER, the electrochemical current density should be as high as possible. We, therefore, immobilized more S-depleted Mo-S NCs on the working electrode to estimate a possible higher current density. Measurement of j_{150} and j_{200} with different amounts of NC catalyst (Figure 3d; polarization curves are shown in Figure S6b) showed a nearly linear dependence on the mass of NC up to 5.26 μg (74.5 $\mu g.cm^{-2}$) for j_{150} and 3.35 μg (47.4 $\mu g.cm^{-2}$) for j_{200}. This gradient thereafter decreased until maximum values of j_{150} = 7.97 $mA.cm^{-2}$ and j_{200} = 33.1 $mA.cm^{-2}$ were reached with 7.17 μg (101 $\mu g.cm^{-2}$) of NCs (Figure 3d). Immobilizing greater amounts of NCs than this resulted in unstable current (reduced during most of the tests) (labeled as 'failed area' in Figure 3d), due to probably the large decrease in electron transport efficiency and catalytically active site numbers (will be further confirmed in Figure 5b). In principle, HER only occurred on the surface of the immoblized NC film. Adding more NCs increased the thickness of catalyst, leading to significant decrease in the electron hopping

efficiency of MoS_2. Electrochemical impedance spectroscopy (EIS) of $MoS_{1.65}$ NCs confirmed that R_{ct} increased from ~200 Ω for 4.78 μg NCs to ~430 Ω for 16.7 μg NCs (Figure 3c).

An Ideal 3D Hybrid Structure for H_2 Production Improvement. The mass limit of increasing current density with $MoS_{1.65}$ NCs and severe degradation of catalytic performance induced by NC's stacking encouraged us to develop a porous 3D $MoS_{1.65}$ structure. A 3D material with active phase on the surface of porous channel has been recognized as a promising structure in many electrochemical processes.[28-30] To achieve this, NCs were immobilized on the graphene-like wall of EG to create a very high exposed surface area. For example, 5.00 μg EG with a specific surface area of 1000 m^2/g can provide 50 cm^2 of surface area, on an electrode of 3 mm diameter, this represents over a 700-fold increase in exposed surface area of catalyst. We prepared 3D EG *via* simple thermal expansion of graphene oxide (GO) containing O-containing groups (see Figure S6d-I and Figure S7a). Nitrogen (N_2) absorption/desorption isotherms of the as-prepared EG (Figure 4a) show the presence of macro- (~42-1050 nm; Figure S6e-f) and meso-scale pores, and Brunaue-Emmett-Teller (BET) surface area of around 450 $m^2.g^{-1}$. This is confirmed by scanning electron microscopy (Figure 4b; Figure S6e-f) and the calculated mesopore diameter (4.6 nm) (Figure 4a inset) using the Barrett-Joyner-Halenda (BJH) method (see Supporting Information for more details about all these results).

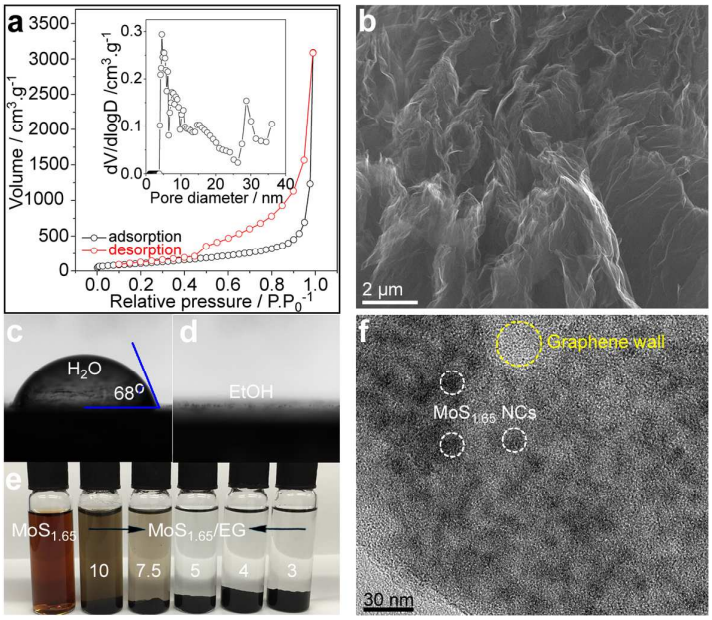

Figure 4. (a) N_2 adsorption/desorption isotherms and BJH pore size distribution (inset), and SEM image (b), of as-prepared EG. (c,d) Contact angle measurements on $MoS_{1.65}$ film with (c) water and (d) EtOH droplet at room temperature. (e) Photographs of 478 μg.mL^{-1} $MoS_{1.65}$ dispersed in H_2O/EtOH (95:5 volume ratio), and $MoS_{1.65}$/EG prepared from 3 mL NC suspension originally made by adding 2.5 mg EG to 10, 7.5, 5, 4 or 3 mL of 478 μg/mL NCs (as labeled) after standing for 24 h. (f) Typical TEM image of the graphene wall of $4MoS_{1.65}$/EG.

On the basis of this preparation, we dispersed $MoS_{1.65}$ NCs in H_2O/EtOH solvent (95:5 volume ratio) to a concentration of ~478 μg.mL^{-1} (see Method and Materials, and Captions of Figure S5f-g for the concentration confirmation). $MoS_{1.65}$ NCs were highly dispersable in EtOH with near zero contact angle but only slightly wettable in H_2O with a contact angle of 68^o (Figure 4c-d), similar to the case of water on EG (Figure S6d inset). Our chosen H_2O/EtOH volume ratio allowed dispersion of NCs and made EG very wettable while making NC adsorption onto EG favourable through reducing the total surface energy of the system. We mixed 2.5 mg EG with different volumes of $MoS_{1.65}$ NC suspension (10, 7.5, 5, 4 and 3 mL; sonication and shaking for 20 mins). After being left to stand for 24 h, the samples with higher concentrations of EG became almost completely clear (Figure 4e), indicating that NCs had penetrated into EG pores

and been readily adsorbed onto EG, with over 98% NCs adsorbed for the 3, 4, and 5 mL NC suspensions (Figure S5h). Mixing 4 mL (rather than 10, 7.5, 5 and 3 mL) NC suspension with 2.5 mg EG to prepare $4MoS_{1.65}$/EG appeared to be optimal for the preparation of NC/EG catalyst (we define '$x$$MoS_{1.65}$/EG' as the catalyst prepared from x mL NCs and 2.5 mg EG; see Supporting Information for how to optimize this preparation). Transmission electron microscopy of $4MoS_{1.65}$/EG catalyst confirmed that the loaded NCs were uniformly dispersed/distributed over the walls of EG (Figure 4f).

Catalytic Performance of 3D Structured S-Depleted Mo-S NCs. We then evaluated the electrochemical HER performance of $4MoS_{1.65}$/EG, in which 4.78 μg of $MoS_{1.65}$ NCs in 10 μL (NCs concentration was confirmed as ~478 $\mu g.mL^{-1}$, previously) of solvent was immobilized on a glassy carbon electrode. The HER with this catalyst began at exceptionally low cathodic voltages ranging from 15-30 mV, giving η around of 50-70 mV, indicating remarkable improvement compared to the case of using pure $MoS_{1.65}$ NCs containing identical total mass of NC (4.78 μg, Figure 3a). Although the Tafel slope for $4MoS_{1.65}$/EG obtained from the polarization curve (Figure 3a; 38 mV/decade in Figure 3b) was higher than the case of $MoS_{1.65}$ NCs with lower mass (~1.2 μg, 29 mV/decade, Figure 3b), it was still close to the value (34 mV/decade) we measured for Pt and lower than that in the case of pure $MoS_{1.65}$ NCs (42 mV/decade) containing identical total mass of NC (4.78 μg, Figure 3b), suggesting that NCs stacking with more NCs had been alleviated. Values of j_{150} and j_{200} (derived from polarization curves, Figure S6c) for EG-loaded $MoS_{1.65}$ NCs were significantly greater than in the case of $MoS_{1.65}$ NCs alone (Figure 5a; derived from the polarization curves in Figure S6b) with identical mass loading of catalyst. The nearly linear dependence of j_{150} and j_{200} upon efficient catalyst mass (*defined as the mass of NCs contained in catalyst materials*) for $4MoS_{1.65}$/EG was also

extended to larger mass values than in the case of $MoS_{1.65}$ alone (Figure 5a). The slight sub-linear dependence of j_{200} above 2.39 μg (33.8 μg.cm^{-2}) of catalyst was likely to be due to the observed rapid H_2 bubble generation. The resistance R_{ct} for$4MoS_{1.65}$/EG was 138 Ω (4.78 μg, cf. 200 Ω for identical efficient catalyst mass of pure $MoS_{16.5}$ NCs) and increasing this to 16.7 μg (236 μg.cm^{-2}) $4MoS_{1.65}$/EG saw R_{ct} reduction further to 88 Ω, in contrast to the previously described behaviour with pure $MoS_{1.65}$ NCs (Figure 3c), suggesting that NCs in $4MoS_{1.65}$/EG had been dispersed and did not stack significantly.

Double layer capacitance (C_{dl}) was calculated from cyclic voltammetry (CV; Figure S8) of $MoS_{1.65}$ NCs, EG and $4MoS_{1.65}$ NCs/EG (Figure 5b,c), based on previously reported methods,[14,31] to provide a measure of the density of catalytically active sites and give direct view of the stacking alleviation by EG. The response as a function of pure $MoS_{1.65}$ NC mass showed three distinct regions of behavior (Figure 5b): *I.* linear increase of C_{dl} for NC mass up to 2.39 μg (33.8 μg.cm^{-2}), indicating limited NC stacking; *II.* sub-linear increase in C_{dl} with NC mass up to 7.17 μg (101 μg.cm^{-2}), suggesting that NC stacking and agglomeration was more prevalent; and *III.* decreasing C_{dl} with increasing NC mass, indicating NC stacking highly suppressed catalytic activity (also see Figure 3c, increase in R_{ct} when NC mass was increased to 16.7 μg, or 236 μg.cm^{-2}). In contrast, C_{dl} for $4MoS_{1.65}$/EG increased linearly with all NC mass values tested (Figure 5c; up to 23.9 μg, or 338 μg.cm^{-2}). The contribution to C_{dl} of $4MoS_{1.65}$/EG by EG only was also determined (Figure 5c) and deducted from that of $4MoS_{1.65}$/EG so as to determine the actual increase in C_{dl} caused by the catalyst loading only (Figure 5c; see Supporting Information for how to determine the contribution to C_{dl} of $4MoS_{1.65}$/EG from EG). This represents the catalytically active surface area and density of catalytically active sites in $4MoS_{1.65}$/EG. Its linear

increase with catalyst mass indicates that adding more $4MoS_{1.65}$/EG did not generate further NCs stacking.

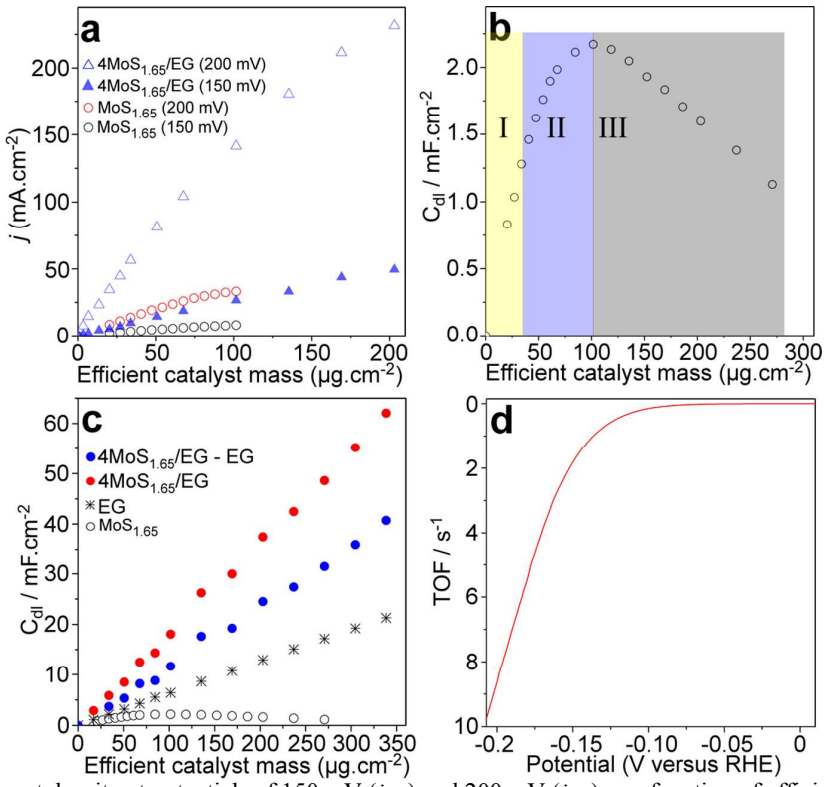

Figure 5. (a) Current density at potentials of 150 mV (j_{150}) and 200 mV (j_{200}) as a function of efficient catalyst mass of $MoS_{1.65}$ NCs and $4MoS_{1.65}$/EG. **(b)** Dependence of double layer capacitance (C_{dl}) on mass of $MoS_{1.65}$ NCs. **(c)** C_{dl} as a function of efficient catalyst mass of $4MoS_{1.65}$/EG and equivalent plots for pure $MoS_{1.65}$ NCs, EG only and calculated $4MoS_{1.65}$/EG – EG capacitance. C_{dl} of a bare glassy carbon electrode was negligible, and set to zero. **(d)** Calculated turnover frequency (TOF) of $4MoS_{1.65}$/EG catalysts at pH≈0.

Although loading $MoS_{1.65}$ NCs on EG did not give a super low Tafel slope (29 mV/decade) achieved by low mass NCs alone (~1.2 µg), the catalytic performance of this hybrid structure was still much better than most of the other MoS_2 based catalysts, and highly suitable for HER with large production. We have achieved very high j_{150} = 49.5 mA/cm^2 and j_{200} = 232 mA/cm^2 with $4MoS_{1.65}$/EG with efficient catalyst mass (the mass of NCs) of ~14.3 µg (202.4 µg.cm^{-2}, Figure 5a; polarization curves are shown in Figure S6c), which is almost impossible to be

obtained by $MoS_{1.65}$ NCs alone on a same area electrode (Figure 3d). This H_2 production efficiency is at least 1-2 orders of magnitude greater than in the cases of most of the other MoS_2-based catalysts of similar mass (Table S2). Increasing the catalyst mass further might, in principle, offer even greater H_2 production efficiencies but we found that the large amount of H_2 generation desquamated the catalyst from the electrode. The $4MoS_{1.65}$/EG catalyst was stable in acid media (Figure S7b-c) with negligible loss of current density (Figure S7d, durability test of 3000 cycles). The η (50-70 mV), Tafel slope (38 mV/decade), and current density under zero potential (j_0) ($j_0 = 5.63\times10^{-3}$ mA.cm^{-2}, derived from Figure 3a) for $4MoS_{1.65}$/EG were much better than in the cases of most of the other MoS_2 based catalysts (*e.g.* Pt and O doped MoS_2,[16,26] monolayered MoS_2,[7] metallic nanosheets,[12] vertically aligned MoS_2 nanofilm,[4] defect rich ultrathin MoS_2 nanosheets,[6] surface engineered MoS_2,[3] amorphous MoS_3 film,[31] monolayered MoS_2 on Au foil,[11] and graphene supported MoS_2 nanoparticles)[14] which typically exhibited η from 100-200 mV, Tafel slopes of 50-145 mV/decade (with very few close to 40 mV/decade) and j_0 from $10^{-8} - 6.9\times10^{-4}$ mA.cm^{-2}. Catalyst mass-dependent current densities for $4MoS_{1.65}$/EG became j'_{150}= 300.26 μA.μg^{-1} (4.25mA.cm^{-2}.μg^{-1}) and j'_{200}= 2.20 mA.μg^{-1} (31.2 mA.cm^{-2}.μg^{-1}) (derived from the initial linear region of Figure 5a), which were also considerably larger than in the other cases (Table S2). More directly, the calculated electrochemical turnover frequency (TOF; rate of H_2 molecule generation per catalytic site; the calculation was carried out based on previously reported methods for Mo-S materials)[31] for $4MoS_{1.5}$/EG was 0.15, 1.86 and 8.74 s^{-1} at 100, 150 and 200 mV potentials, respectively (Figure 5d; Figure S9; using efficient catalyst massof 2.39 μg), which was > 1 order of magnitude greater than in the case of most of the other MoS_2-based catalysts (Table S1).[1,3,4,6,7,11,14,16,31,32]

Our density functional theory (DFT) calculations on monolayered NCs reveal a metallic shell around the edge of the NCs (Figure 2). This is unlike monolayered sheets of MoS_2 and will improve charge mobility further. XPS of the NCs confirmed the existence of this metallic phase in MoS_2 NCs (Figure S3b, showing 5.57% Mo contribution). XPS of S-depleted ($MoS_{1.65}$) NCs showed an increased number of metallic sites (Figure 1e, 11.8% Mo contribution). Hydrogen adsorption and TOF of these exposed sites on the basal plane, in principle, are also better than for traditional edge sites.[33] The proportion of metallic phase increased further when the S-depleted NCs were immobilized onto EG (Figure S7b, 23.3% Mo contribution). Similarly to internal defect levels introduced by S-depletion (see Figure 2), we found that O doping (S oxidized) formed upon binding with EG (Figure S7a-c), which, according to Xie *et al*, could enhance the intrinsic conductivity of MoS_2-based catalysts due to the internal defect levels.[26] EIS (Figure 3c) for the materials showed a decrease in resistance when moving from MoS_2 to $MoS_{1.65}$ NCs, and further decreases with $4MoS_{1.65}$/EG. All these reasons made $4MoS_{1.65}$/EG be a better catalyst than MoS_2 and $MoS_{1.65}$ NCs when NC's immobilization mass was > 1.2 μg. In the case of $4MoS_{1.65}$/EG, we also recognized that the super catalytic performance of pure S-depleted NCs (*e.g.* Tafel slope of 29 mV/decade) has not been fully developed, which means some NCs stacking still remained and slightly degenerated catalytic performance (*e.g.* Tafel slope increased to 38 mV/decade), when large amounts of $MoS_{1.65}$ NCs were used. Nevertheless, this hybrid structure is already highly suitable for HER with high production.

CONCLUSIONS

We have demonstrated how the chemical and structural design on Mo-S monolayers can improve dramatically catalysis of HER. We exfoliated and disintegrated monolayered 2H MoS_2 NCs (2-25 nm) from bulk flakes with a high yield (31 wt%) to obtain stable NC suspensions. Unlike

monolayered sheets, the MoS_2 NCs consisted of metallic edges and shells, and a semiconducting core, making their catalytic performance (for electrochemical HER; *e.g.* overpotential of 120-140 mV and Tafel slope of 51 mV/decade) become much better than that of monolayered sheets. However, the majority of Mo sites are on the basal plane of MoS_2 NCs and remain catalytically inactive away from the edge. S-depleting the MoS_2 NCs with a cation exchange resin activated surface Mo for HER and produced NCs with super and stable catalytic performance for HER, *e.g.* overpotential of 60-75 mV and Tafel slope of ~29 mV/decade. This compares with overpotential of > 120 mV and Tafel slope of ~50-150 mV/decade of various other thin and defected Mo-S NCs.[3,6,7,25,26,31] We have found that increased production of H_2 cannot be achieved *via* immobilizing more (or multilayers of) Mo-S materials onto an electrode of fixed size, because the HER only occurs on the topmost layer of the catalyst and the charge mobility decreases dramatically. Highly efficient HER with a Mo-S catalyst demands a single Mo-S layer with a high surface area, which is challenging with a traditional 2D film based catalyst. We have demonstrated that this challenge can be largely overcome by building a 3D hybrid structure of Mo-S based catalyst. A simple preparation method allowed S-depleted Mo-S NCs to be loaded onto a porous 3D graphene-like material (expanded graphene oxide/EG) to create an exceptionally high surface area catalyst structure without significant Mo-S NC agglomeration or stacking. Although catalytic performance of the S-depleted Mo-S NCs has not been fully developed, the prepared hybrid catalyst has already shown excellent performances on HER, *e.g.* overpotentials of 50-70 mV, Tafel slope of 38 mV/decade, TOF of 8.74 s^{-1} at 200 mV, and current density at 0 mV of 5.63×10^{-3} $mA.cm^{-2}$ with < 4.78 μg NCs, which are over one order of magnitude better than in the cases of most of the other MoS_2-based catalysts. A very high H_2 production was also achieved (current densities of 49.5 and 232 mA/cm^2 at overpotentials of 150

and 200 mV) using ~14.3 μg S-depleted Mo-S NCs. This performance could be further improved using other existing approaches to modify Mo-S materials (*e.g.* chemical doping, further surface modification of the S-depleted NCs, and binding with other metal based catalysts), and to further avoid the NC stacking.[16,32,34] Further improvement of H_2 production is limited by the desquamation of catalyst due to the rapid generation of large H_2 bubbles. Such limits, however, can be overcome rather easily by using other 3D graphene (*e.g.* 3D graphene grown on metal substrates, crosslinked porous graphene from graphene oxide gel) or other conductive materials (*e.g.* conductive ceramics with cellular architectures and porous polypyrrole polymer).[35]

METHOD AND MATERIALS

Preparation of Monolayered MoS_2 NCs and S Depletion. Monolayered MoS_2 NCs were prepared followed on our previously reported method.[18-20] Briefly, around 0.6 g K was put into a stoppered Pyrex tube with a vacuum connection, followed by adding 1 g MoS_2 flakes. The two materials were mixed by gently shaking the Pyrex tube. The tube was heated to 180-190 ^oC and held for >4 h. After cooling the tube to room temperature, the vacuum pump was turned off. The bottom of the Pyrex tube was placed in a room temperature water bath in an ultrasonic vibrator (Bandelin Sonorex RK-100H, 320 W). The Pyrex tube was then rapidly vented to air. Under ultrasonic stimulation, the stop cover of the tube was removed and 50 mL ethanol added. Upon all visible K disappearing from the surface of the solution, 50 mL H_2O was added to the tube. The tube was kept in the ultrasonic bath for 2 h. A faint yellow solution containing MoS_2 NCs was separated from the residual solid MoS_2 by centrifugation. Then the collected suspension was heated in an oven to evaporate ethanol. The remaining K ions in the solution and partial surface S of the NCs were removed by flowing the half prepared solution through a funnel filled with

cation exchange resin (with ~5 cm filling height). Smelly H_2S (verified by our GC test with BID detector) was produced and the faint yellow suspension became reddish brown. MoS_2 NCs were also prepared by removal of the remaining K ions with dialysis tubing for characterizations.

Preparation of GO and Expansion of GO. Graphene oxide (GO) was prepared followed the modified Hummer's method previously reported by us.[36] Briefly, 2 g of graphite flakes (Nacalai Tesque, product No.: 17346-25) and 1.5 g $NaNO_3$ were added to a 800 mL wide neck flask, followed by 150 mL H_2SO_4 (95.0-98.0%) while stirring. The flask was kept at around 35 ^oC using a water bath and 9 g $KMnO_4$ added after 1 h. After further stirring for 24 h at around 35 ^oC, 280 mL 5% H_2SO_4 was added to the mixture and the temperature was increased to 85-95 ^oC using an oil bath. The mixture was stirred for another 2 h, cooled down in the flask to around 60 ^oC, and then 15 mL H_2O_2 (30 wt%) was added to the mixture. The mixture was collected after 2h further stirring. Impurities were removed by washing the mixture with diluted HCl. The resulting GO was gently diluted and stirred (violent stirring must be avoided as this can exfoliate GO sheets and affect the following separation). GO sol was collected with a centrifuge at 6000 RPM several times until the pH of the suspension was up to 6 at room temperature. GO sol was dried on the surface of a watchglass to form a thin GO paper which was then cut into small pieces (Figure S6d). Some GO pieces were put into a hot alumina crucible (375-425 ^oC, on hot plate), which was then covered by a metal plate. Expansion of the GO occurred within 3-10 seconds (accompanied by clear expansion sounds). The crucible was then removed from the hot plate and cooled to < 300 ^oC. Finally, the expanded graphene oxide (EG) was transferred onto a clean watch glass and was ready for use.

Characterizations. X-ray diffraction (XRD) was performed using a Philips PW 1830 powder diffractometer (Cu Kα, wavelength ~ 0.154 nm, with a scanning step of 2 ^{o}/min) using a constant

amount of the material. Photoluminescence (PL) spectra were recorded using a Hitachi F-4500 Fluorescence Spectrophotometer at 20 ^{o}C. UV/Vis spectra were recorded using a Shimadzu-3600 UV-VIS-NIR spectrophotometer. Raman spectra were recorded on a Renishaw In Plus laser Raman spectrometer with an excitation wavelength λ_{exc} = 514.5 nm. FT-IR was performed on a Shimadzu IR-Tracer-100 FT-IR spectrometer. Scanning electron microscopy (SEM) was performed using a commercial Nova 600 NanoSEM without any additional conductive surface coating. X-ray photoelectron spectroscopy (XPS) was performed on a Kratos AXIS Nova X-ray photoelectron spectrometer with an excitation source of Al K_{α}. The binding energy of XPS was calibrated based on C1s (284.6 eV). Atomic force microscopy (AFM) was performed using a VEECO Dimension 3100 system in tapping mode with a scan rate of 1 Hz (with samples placed on mica substrates). Transmission electron microscopy (TEM) images were obtained using a JEM-2100 200 kV (EDS were also taken during this TEM characterization) and a JEOL 2010F transmission electron microscope with a field emission gun operated at 200 kV. The wettability of the sample was determined using a contact angle goniometer.

Calculation of The Yield and Mass of Monolayered Mo-S NCs. Direct determination of the mass of catalyst for electrochemical tests is technically difficult. However, we prepared highly pure S-depleted NCs with half MoS_2 NC suspension. Half S-depleted NCs were dried and weighed. The UV/Vis absorption coefficiency and Beer-Lambert plot (Figure S5f&g) at one most characteristic absorption peak (207 nm) of the remained S-depleted NCs was determined. We then prepared a 478 $\mu g.mL^{-1}$ concentration of S-depleted NCs as the standard for most of the measurement. NCs with high concentrations (*e.g.* 2, 3 and 4 times greater than 478 $\mu g.mL^{-1}$) were also held for immobilization of larger quantities of NCs. More dilute suspensions were also used and their concentration was verified using the Beer-Lambert plot in Figure S5g. We

prepared 3D graphene supported NCs with 2.5 mg EG and S-depleted NCs with different amount (*e.g.* 3, 4, 5, 7.5 and 10 mL). Over 98% (confirmed by UV/Vis spectroscopy in Figure S5h) NCs had been adsorbed by 3D graphene with NC addition amount of 3, 4 and 5 mL. We used $4MoS_{1.65}$/EG (4 mL S-depleted NCs and 2.5 mg EG) for the measurement, and reasons for this choice are explained in the Supporting Information. For each test, the efficient catalyst (NC) mass can be simply determined by the volume used for immobilization. To confirm the yield of MoS_2 NCs, it was hard to weigh the dialyzed sample since lots of NCs were lost during the dialysis. However, we determined the mass of prepared MoS_2 (MW: 160.07 g/mol) NCs based on the mass of S-depleted $MoS_{1.65}$ NCs (MW: 148.85 g/mol) as follows:

$$M_1 = 2 \times 160.07 \times \frac{2M_2}{148.85}$$

where M_1 and M_2 are respectively the mass of produced MoS_2 NCs, and the mass of weighed S-depleted $MoS_{1.65}$ NCs (half of the MoS_2 NCs remained, and half were treated to deplete partial S, and half of the S-depleted NCs were dried and weighed). On the basis of the mass of the S-depleted $MoS_{1.65}$ NCs, the concentration of the remained MoS_2 NCs was also confirmed for different electrochemical measurements.

ASSOCIATED CONTENT

Supporting Information

Supplementary methods and additional materials, characterizations are available free of charge *via* the Internet at http://pubs.acs.org.

AUTHOR INFORMATION

Corresponding Author

*d.allwood@sheffield.ac.uk

*s.zhang@exeter.ac.uk

Author Contributions

LL conducted the experimental work with assistance from YW, while LL also proposed the research; NM, PG and ZS performed the density functional theory calculations; SZ and DAA provided supervision and oversight to the experimental work, and drafted the manuscript with LL.

Notes

The authors declare no competing financial interest.

ACKNOWLEDGEMENT

This work was supported by the University of Sheffield (Faculty Scholarship) and the University of Exeter (Start-up Fund). We thank the National EPSRC XPS Users' Service (NEXUS) at the Newcastle University (UK) for the assistance with XPS characterizations. We thank Dr. David W. Horsell at the University of Exeter for the assistance on contact angle measurements.

REFERENCES

(1) Hinnemann, B.; Moses, P. G.; Bonde, J.; Jøergensen, K. P.; Nielsen, J. H.; Horch, S.; Chorkendorff, I.; Nørskov, J. K. Biomimetic Hydrogen Evolution: MoS_2 Nanoparticles as Catalyst for Hydrogen Evolution. *J. Am. Chem. Soc.* **2005**, *127*, 5308-5309.

(2) Karunadasa, H. I.; Montalvo, E.; Sun, Y.; Majda, M.; Long J. R.; Chang, C. J. A Molecular MoS_2 Edge Site Mimic for Catalytic Hydrogen Generation. *Science* **2012**, *335*, 698-702.

(3) Kibsgaard, J.; Chen, Z.; Reinecke, B. N.; Jaramillo, T. F. Engineering the Surface Structure of MoS_2 to Preferentially Expose Active Edge Sites for Electrocatalysis. *Nat. Mater.* **2012**, *11*, 963-969.

(4) Wang, H.; Lu, Z.; Xu, S.; Kong, D.; Cha, J. J.; Zheng, G.; Hsu, P.-C.; Yan, K.; Bradshaw, D.; Prinz, F. B.; Cui, Y. Electrochemical Tuning of Vertically Aligned MoS_2 Nanofilms and Its Application in Improving Hydrogen Evolution Reaction. *Proc. Natl. Acad. Sci. USA* **2013**, *110*, 19701-19706.

(5) Jaramillo, T. F.; Jøergensen, K. P.; Bonde, J.; Nielsen, J. H.; Horch, S.; Chorkendorff, I. Identification of Active Edge Sites for Electrochemical H_2 Evolution from MoS_2 Nanocatalysts. *Science* **2007**, *317*, 100-102.

(6) Xie, J.; Zhang, H.; Li, S.; Wang, R.; Sun, X.; Zhou, M.; Zhou, J.; Lou, X. W. D.; Xie, Y. Defect-rich MoS_2 Ultrathin Nanosheets with Additional Active Edge Sites for Enhanced Electrocatalytic Hydrogen Evolution *Adv. Mater.* **2013**, *25*, 5807-5813.

(7) Yu, Y.; Huang, S.-Y.; Li, Y.; Steinmann, S. N.; Yang, W.; Cao, L. Layer-Dependent Electrocatalysis of MoS_2 for Hydrogen Evolution. *Nano Lett.* **2014**, *14*, 553-558.

(8) Vesborg, P. C. K.; Seger, B.; Chorkendorff, I. Recent Development in Hydrogen Evolution Reaction Catalysts and Their Practical Implementation. *J. Phys. Chem. Lett.* **2015**, *6*, 951-957.

(9) Voiry, D.; Yang, J.; Chhowalla, M. Recent Strategies for Improving the Catalytic Acitivity of 2D TMD Nanosheets Toward the Hydrogen Evolution Reaction. *Adv. Mater.* **2016**, *28*, 6197-6206.

(10) Voiry, D.; Fullon, R.; Yang, J.; Silva, Silva, C. C. C. e; Kappera, R.; Bozkurt, I.; Lagos, M. J.; Batson, P. E.; Gupta, G.; Mohite, A. D.; Dong, L.; Er, D.; Shenoy, V. B.; Asefa, T.; Chhowalla, M.; The Role of Electronic Coupling between Substrate and 2D MoS_2 Nanosheets in Electrocatalytic Production of Hydrogen. *Nat. Mater.* **2016**, doi:10.1038/nmat4660.

(11) Shi, J.; Ma, D.; Han, G.-F.; Zhang, Y.; Ji, Q.; Gao, T.; Sun, J.; Song, X.; Li, C.; Zhang, Y.; Lang, X-Y.; Zhang, Y.; Liu, Z. Controllable Growth and Transfer of Monolayer MoS_2 on Au Foils and Its Potential Application in Hydrogen Evolution Reaction. *ACS Nano* **2014**, *8*, 10196-10204.

(12) Lukowski, M. A.; Daniel, A. S.; Meng, F.; Forticaux, A.; Li, L.; Jin, S. Enhanced Hydrogen Evolution Catalysis from Chemically Exfoliated Metallic MoS_2 Nanosheets. *J. Am. Chem. Soc.* **2013**, *135*, 10274-10277.

(13) Voiry, D.; Salehi, M.; Silva, R.; Fujita, T.; Chen, M.; Asefa, T.; Shenoy, V. B.; Eda, G.; Chhowalla, M. Conducting MoS_2 Nanosheets as Catalyst for Hydrogen Evolution Reaction. *Nano Lett.* **2013**, *13*, 6222-6227.

(14) Li, Y.; Wang, H.; Xie, L.; Liang, Y.; Hong, G.; Dai, H. MoS_2 Nanoparticles Grown on Graphene: An Advanced Catalyst for the Hydrogen Evolution Reaction. *J. Am. Chem. Soc.* **2011**, *133*, 7296-7299.

(15) Ren, X.; Ma, Q.; Fan, H.; Pang, L.; Zhang, Y.; Yao, Y.; Ren, X.; Liu, S. A Se-doped MoS_2 Nanosheet for Improved Hydrogen Evolution Reaction. *Chem. Commun.* **2015**, *51*, 15997-6000.

(16) Deng, J.; Li, H.; Xiao, J.; Tu, Y.; Deng, D.; Yang, H.; Li, J.; Ren, P.; Bao, X. Triggering The Electrocatalytic Hydrogen Evolution Activity of the Inert Two-Dimensional MoS_2 Surface *via* Single-Atom Metal Doping. *Energy Environ. Sci*. **2015**, *8*, 1594-1601.

(17) Le, D.; Rawal T. B.; Rahman, T. S. Single-Layer MoS_2 with Sulfur Vacancies: Structure and Catalytic Application. *J. Phys. Chem. C* **2014**, *118*, 5346-5351.

(18) Lin, L.; Zhang, S. Creating High Yield Water Soluble Luminescent Graphene Quantum Dots *via* Exfoliating and Disintegrating Carbon Nanotubes and Graphite Flakes. *Chem. Commun*. **2012**, *48*, 10177-10179.

(19) Lin, L.; Xu, Y.; Zhang, S.; Ross, I. M.; Ong A. C. M.; Allwood, D. A. Fabrication of Luminescent Monolayered Tungsten Dichalcogenides Quantum Dots with Giant Spin-Valley Coupling. *ACS Nano* **2013**, *7*, 8214-8223.

(20) Lin, L.; Xu, Y.; Zhang, S.; Ross, I. M.; Ong A. C. M.; Allwood, D. A. Fabrication and Luminescence of Monolayered Boron Nitride Quantum Dots. *Small* **2014**, *10*, 60-65.

(21) Jacobson, A. J.; Nazar, L. F. in *Intercalation Chemistry. Encyclopedia of Inorganic Chemistry* (WILEY-VCH, Weinheim, **2006**).

(22) Eda, G.; Yamaguchi, H.; Voiry, D.; Fujita, T.; Chen, M.; Chhowalla, M. Photoluminescence from Chemically Exfoliated MoS_2. *Nano Lett.* **2011**, *11*, 5111-5116.

(23) Wilcoxon, J. P.; Newcomer, P. P.; Samara, G. A. Synthesis and Optical Properties of MoS_2 and Isomorphous Nanoclusters in the Quantum Confinement Regime. *J. Appl. Phys.* **1997**, *81*, 7934-7944.

(24) Lee, C. Anomalous Lattice Vibrations of Single- and Few-Layer MoS_2. *ACS Nano* **2010**, *4*, 2695-2700.

(25) Baker, M. A.; Gilmore, R.; Lenardi, C.; Gissler, W. XPS Investigation of Preferential Sputtering of S from MoS_2 and Determination of MoS_x Stoichiometry from Mo and S Peak Positions. *Appl. Surf. Sci*. **1999**, *150*, 255-262.

(26) Xie, J.; Zhang, J.; Li, S.; Grote, F.; Zhang, X.; Zhang, H.; Wang, R.; Lei, Y.; Pan, B.; Xie, Y. Controllable Disorder Engineering in Oxygen-Incorporated MoS_2 Ultrathin Nanosheets for Efficient Hydrogen Evolution. *J. Am. Chem. Soc.* **2013**, *135*, 17881-17888.

(27) Shin, S.; Jin, Z.; Kwon, D. H.; Bose, R.; Min, Y.-S. High Turnover Frequency of Hydrogen Evolution Reaction on Amorphous MoS_2 Thin Film Directly Grown by Atomic Layer Deposition. *Langmuir* **2015**, *31*, 1196-1202.

(28) Li, X.; Dhanabalan A.; Wang, C. Enhanced Electrochemical Performance of Porous NiO-Ni Nanocomposite Anode for Lithium Ion Batteries. *J. Power Sources* **2011**, *196*, 9625-9630.

(29) Li, X.; Dhanabalan A.; Gu, L.; Wang, C. Three-Dimensional Porous Core-Shell Sn@Carbon Composite Anodes for High-Performance Lithium-Ion Battery Applications. *Adv. Energy Mate*r. **2012**, *2*, 238-244.

(30) Chabi, S.; Peng, C.; Hu, D.; Zhu, Y. Ideal Three-Dimensional Electrode Structures for Electrochemical Energy Storage. *Adv. Mater*. **2014**, *26*, 2440-2445.

(31) Merki, D.; Fierro, S.; Vrubel, H.; Hu, X. Amorphous Molybdenum Sulfide Films as Catalysts for Electrochemical Hydrogen Production in Water. *Chem. Sci.* **2012**, *2*, 1262-1267.

(32) Lai, F.; Miao, Y.-E.; Huang, Y.; Zhang, Y.; Liu, T. Nitrogen-Doped Carbon Nanofiber/Molybdenum Disulfide Nanocomposites Derived from Bacterial Cellulose for High-Efficiency Electrocatalytic Hydrogen Evolution Reaction. *ACS Appl. Mater. Inter.* **2016**, *8*, 3558-3566.

(33) Li, H.; Tsai, C.; Koh, A. L.; Cai, L.; Contryman, A. W.; Fragapane, A. H.; Zhao, J.; Han, H. S.; Manoharan, H. C.; Abild-Pedersen, F.; Nørskov, J. K.; Zheng, X. Activating and Optimizing MoS_2 Basal Planes for Hydrogen Evolution Through the Formation of Strained Sulphur Vacancies. *Nat. Mater.* **2016**, *15*, 48-53.

(34) Gao, M.; Liang, J.; Zheng, Y.; Xu, Y.; Jiang, J.; Gao, Q.; Li, J.; Yu, S. An Efficient Molybdenum Disulfide/Cobalt Diselenide Hybrid Catalyst for Electrochemical Hydrogen Generation. *Nat. Commun.* **2014**, *6*, 5982.

(35) Wang, T.; Zhuo, J.; Du, K.; Chen, B.; Zhu, Z.; Shao, Y. Electrochemically Fabricated Polypyrrole and MoS_x Copolymer Films as a Highly Active Hydrogen Evolution Electrocatalyst. *Adv. Mater.* **2014**, *26*, 3761-3766.

(36) Lin, L.; Zheng, X.; Zhang, S.; Allwood, D. Surface Energy Engineering in the Solvothermal Deoxidation of Graphene Oxide. *Adv. Mater. Interfaces* **2014**, *1*, 1300078.